LLNL-JRNL-750994

LAWRENCE
LIVERMORE
NATIONAL
LABORATORY

Capturing Phase Behavior of Ternary Lipid Mixtures with a Refined Martini Coarse-grained Force Field

T. S. Carpenter, C. A. Lopez, C. Neale, C. Montour, H. I. Ingolfsson, F. Di Natale, F. C. Lightstone, S. Gnanakaran

May 8, 2018

Journal of Chemical Theory and Computation

Disclaimer

This document was prepared as an account of work sponsored by an agency of the United States government. Neither the United States government nor Lawrence Livermore National Security, LLC, nor any of their employees makes any warranty, expressed or implied, or assumes any legal liability or responsibility for the accuracy, completeness, or usefulness of any information, apparatus, product, or process disclosed, or represents that its use would not infringe privately owned rights. Reference herein to any specific commercial product, process, or service by trade name, trademark, manufacturer, or otherwise does not necessarily constitute or imply its endorsement, recommendation, or favoring by the United States government or Lawrence Livermore National Security, LLC. The views and opinions of authors expressed herein do not necessarily state or reflect those of the United States government or Lawrence Livermore National Security, LLC, and shall not be used for advertising or product endorsement purposes.

INTRODUCTION

Lipid rafts are relatively small, heterogeneous, highly dynamic, cholesterol-rich domains that play important roles in the regulation of membrane protein activity[1-5]. The conditions underlying the formation of distinguishable lipid phases have been the subject of intense research for decades[6-7]. *In vitro* studies at 298 K with biologically relevant cholesterol concentrations show the spontaneous emergence of a liquid-ordered (L_o) phase that features a rich condensation of cholesterol and saturated, high T_m lipids, which separates from a liquid-disordered (L_d) phase that is depleted of cholesterol and enriched with unsaturated, low T_m lipids[8-9].

The structure of lipid domains[10-11] can now be experimentally visualized. Fluorescently labeled lipids with affinities for L_o domains similar to those of unlabeled lipids are enriched near proteins that localize to lipid rafts in living cells[12-14]. Reciprocally, single-particle-tracking measurements show that these associations vanish when minor changes are made in the lipid or protein that weaken their physical bases for raft association[15-17]. In addition, new evidence suggests the presence of transient nanometer-size domains in eukaryotic cells at physiological temperatures[18-19], as well as reversible phase separation in biological lipid membranes at lower temperatures[20-21]. In other studies, super-resolution microscopy has shown that raft markers co-localize with clustered B-cell receptors at 50-100 nanometer resolution[22-23], and the formation of lipid nanodomains has been implicated in viral entry[24] and the internalization of bacterial toxins[25-26].

Despite the aforementioned advances in the detection of lipid rafts, the characterization of small domains still remains difficult[20], and the structural and dynamic complexity of the plasma membrane has led to much controversy regarding the existence and relevance of these domains

in living cells[27-28]. For these reasons molecular dynamics (MD) simulations have increasingly become a useful tool to provide spatial and temporal quantification of membrane substructures at multiple resolutions.

Recent work has shown that it is possible to track the evolution of lipid domain formation using all atom (AA) computer simulations[29-30]. Specifically, at experimentally relevant temperatures, simplified lipid compositions form coexisting L_o and L_d phases within tens of microseconds[29-30]. Although the results of such AA simulations are encouraging, the contemporary computational burden places this approach outside the realm of utility in all but the most exceptional cases. One way to mitigate these computational limitations is to use the Martini coarse-grained (CG) force field[31], which reduces the computational cost by a factor of ~1,000[32]. Pioneering efforts with the Martini CG force field allowed the characterization of not only lipid segregation and lipid phases, but also the relative partitioning of membrane proteins between these phases[33-36]. More recently, Martini has been used in simulations of membranes with lipid compositions of comparable complexity to those found in specific tissues of live cells[37-38].

As outlined above, the benefits of coarse-graining in molecular simulations are clear. Nevertheless, reliable simulations require accurate parameters, and the existing Martini lipid models have two main shortcomings in this area. First, saturated Martini lipids generally fail to reproduce known, gel-liquid, melting transition temperatures[39-40]. As a result, simulated lipid phase separation requires either temperatures that are substantially below experimental separation temperatures or the use of a lipidic component with artificially high levels of acyl-chain unsaturation[33-34]. Second, as a consequence of the modularity of the Martini approach, some commonly used unsaturated lipids do not reproduce experimental temperature-dependent

phase separation. In many ways the hallmark of the Martini model is its modular design criterion, facilitating rapid parameter addition for new chemical species[41]. However, although many of the current Martini lipid parameters are sufficient to guide accurate membrane simulations[31, 39-40], global lipid properties appear to be compromised in some lipid mixtures[42]. Others have shown that some commonly used unsaturated lipids like 1,2-dioleoyl-*sn*-glycero-3-phosphatidylcholine (DOPC) and 1-palmitoyl-2-oleoyl-*sn*-glycero-3-phosphatidylcholine (POPC) do not reproduce experimental temperature-dependent phase separation from saturated lipids and cholesterol (CHOL)[43-45]. To mitigate this limitation, DIPC (dilinoleoylphosphatidylcholine, 18:2,PC) is often used as an alternative low T_m lipid to observe phase separating behavior[33, 46-47]. While DIPC is a good representative lipid to study the mechanism and dynamics of phase separation, we show that with the standard Martini parameters this lipid leads to 'over-separation' in that every mixture that contains all three components (DPPC, DIPC, and CHOL) undergoes phase separation (**Figs. S1 and S2**). Since this mixture phase separates in regions closer to the critical point where the plasma membrane resides, it questions the use of this DIPC to represent biologically relevant lipid mixtures, and thus should not be considered as a direct surrogate for DOPC. In combination, these limitations motivate an improvement for a more experimentally accurate phase-separating Martini-compatible model.

Here, we present a strategy to refine Martini parameters that can greatly improve the phase behavior of a commonly used lipid mixture. Two different re-parameterized sets are presented: one that satisfies the building block philosophy of Martini and one that is optimized purely in a lipid-specific manner. Our approach is designed to maximize the consistency of the new parameters with the larger Martini framework by re-parameterizing only bonded terms of

existing CG bead types. We base this refinement on the results of atomistic simulations of homogeneous lipid bilayers conducted with the CHARMM36 force field[48-49]. We considered a well-studied lipid mixture, both in terms of computations and experiments, DOPC (low T_m), DPPC (high T_m), and CHOL. The resulting refined parameters preserve structural characteristics that are already consistent with the standard Martini[31] for homogeneous lipid bilayers and shift the T_m for DPPC towards the experimentally measured value. Importantly, these refined Martini parameters reproduce the experimentally measured complete phase diagram. The re-parameterization approach for the Martini force field that we present here can be extended to include other lipid species in the future.

METHODS

RE-PARAMETERIZATION STRATEGY. To maximize the compatibility of our refined parameters with those of other molecules available in the Martini force field, we followed the basic philosophy inherent to that model[31, 39]. Therefore, CG bead types and their corresponding non-bonded terms were not modified. Rather, our re-parameterization strategy involved modifying the bonded terms for Martini lipids such that their sampled populations best fit the distributions obtained from a pseudo CG-mapping generated from AA CHARMM36 force field. Distributions of sampled bond and angle terms were collected from these pseudo-CG trajectories and used as target functions in the iterative modification of Martini bonded parameters until a close match was achieved.

PROCEDURE FOR RE-PARAMETERIZATION. AA trajectories were converted into pseudo-CG trajectories using the geometrical projection method published by Wassenar et al.[50] Briefly, the corresponding lipid coordinates for every AA frame were translated into CG coordinates using an orthogonal projection based on the center of mass of pre-defined atomic groups. The procedure was iteratively repeated for every single frame until the whole trajectory was covered. The set of directives for the transformation between CHARMM36 and Martini were updated from the original work and provided as part of the supporting material. From the collected pseudo CG trajectories, bonded and angles distributions were collected and iteratively fitted into the CG representation, until a close match is achieved. The updated list of parameters for both DPPC and DOPC are also provided as appendices.

MARTINI CG MAPPING. In general, the mapping preserved the Martini philosophy of four heavy atoms into one single CG bead[31], except for mapping the unsaturated carbon tails of DOPC. For this particular case, we pre-defined a mapping scheme that condenses up to five carbons into one single bead (see Results). In order to compensate the uneven number of atoms per bead, the bond equilibrium distance between connecting particles required optimization to reproduce the distributions observed in the atomistic simulations. The optimization retained the same number of bonds in the standard Martini force field, however one extra angle was incorporated in order to modulate the orientation of the glycerol moiety in both DPPC and DOPC (see Results). An overview of the atomistic to CG mapping is shown in **Fig. 1A and B**.

AA (CHARMM36) SIMULATION DETAILS. Atomistic systems comprised of a hydrated lipid bilayer with 64 lipids per bilayer leaflet, 50 water molecules per lipid, and 150 mM KCl. Each lipid composition was simulated for 600 ns. Temperatures were 310 K and 323 K for DOPC and DPPC lipids, respectively. Distributions of conformational properties from the final 300 ns per simulation were used to guide the optimization of CG parameters. Additional details, including AA T_m computations, are included in the Supporting Material.

CG SIMULATIONS FOR REPARAMETERIZATION. Initial configurations of CG membrane patches with homogeneous lipids were obtained by CG-mapping the final snapshots of DPPC and DOPC from AA simulations. Thus, CG systems contained 64 lipids per leaflet,

1,600 Martini water beads (50 atomistic water molecules per lipid) and 150 mM NaCl to preserve the ionic strength from AA simulations. Simulations were run with GROMACS[51] version 5.1.2 in combination with the Martini V2.2 force field[31], using its standard (non-polarizable) water model. The newer, refined cholesterol molecule with virtual-sites was also used[52]. We followed a current update in parameters set-up for performing the CG simulations, using the new-ref set[53]. The simulation time-step was 30 fs. Reaction-field electrostatics was used with a Coulomb cut-off of 1.1 nm and dielectric constants of 15 or 0 within or beyond this cut-off, respectively. Lennard-Jones interactions were cut off at 1.1 nm, where the potential was shifted to zero. Constant temperature was maintained at 323 K (DPPC) or 310 K (DOPC) via separate coupling of the solvent (water and ions) and membrane (DPPC or DOPC) components to velocity-rescaling thermostats[54] with relaxation times of 1.0 ps. During equilibration, pressure was semi-isotropically coupled at 1 bar, using Berendsen[55] barostats with relaxation times of 12.0 ps and compressibilities of $3x10^{-4}$ bar^{-1}. After equilibration, Parrinello-Rahman barostats[56] were used. Some analyses used tools provided in the GROMACS package[51].

CG SIMULATIONS TO COMPUTE T_m. To estimate the phase transition temperature, T_m, for DPPC, we followed the protocol described by Marrink *et al.*[57]. Specifically, we constructed a membrane patch consisting of 550 DPPC, 5,800 water molecules (42 water molecules per lipid) and 150 mM NaCl. This system was equilibrated for 0.5 μs at 330 K and instantaneously cooled to 280 K, well below the experimental DPPC T_m (314 K)[58] and the T_m estimated by Marrink *et al.* for standard Martini parameters (295 K)[57]. From these fast quenching simulations, a configuration was selected in which some of the lipids underwent a liquid-gel (L_d to L_β) transition, and the remaining lipids remained in the L_d phase. This mixed-phase configuration

was used for estimating the computational T_m by running simulations at a range of temperatures and quantifying the relative growth of each lipid phase via the measurement of the average area per lipid (APL).

CG SIMULATIONS TO COMPUTE PHASE DIAGRAM. To test the optimized lipid parameters over a wide range of simulation conditions and lipid environments, we completed sweeping studies of the ternary phase diagram for DPPC/DOPC/CHOL at 290, 298, and 310 K. All membranes were set up using the *insane* CG building tool[41]. Each system contained ~3,000 total lipids, ~69,300 CG waters, ~7,700 CG antifreeze particles (10% of the solvent; used to prevent the freezing of water beads), and 150 mM NaCl. The total system size was about 30×30×15 nm and consisted of ~110,000 CG particles. To limit large-scale bilayer undulations, weak position restraints (force constant of 2 kJ/mol/nm^2) were applied in the Cartesian **z** dimension (global bilayer normal) to the phosphate bead of each phospholipid in the bilayer's upper leaflet[59]. Systems were equilibrated by energy-minimization (steepest descent, 1,500 steps) followed by successive simulation using time-steps of 1 fs (for 0.1 ns) and 10 fs (for 1 ns) before initiating 15 μs production simulations with a 35 fs time-step. Accounting for the roughly 4-fold faster diffusion at the Martini CG level[60], this corresponds to ~60 μs of effective sampling. All analyses were averaged over the last 1 μs of each simulation. During system construction, lipidic components were combined in increments of 10% of the total number of membrane lipids to produce 51 separate simulations that scan the phase diagram (**Fig. S3**). The CHOL composition was capped at 50% because cholesterol crystallizes above these concentrations[61]. This culminated in 510 separate simulations, with a total of 7.65 ms of real simulation time. In order to rapidly set up the different system compositions, run and monitor the simulation jobs, we

utilized a new workflow manager named Maestro Workflow Conductor (MaestroWF)[62]. MaestroWF is a Python based tool centered on the core principles of providing users the ability to clearly specify workflows that are both repeatable and portable. The tool also provides a lightweight framework that parses a specification, constructing a directed graph that is used by the backend orchestrator (called the "conductor") to automatically set up, monitor and launch steps in a multistep workflow. Other features that MaestroWF includes are a backend set of adapters for interfacing with multiple simulation job schedulers, as well as a set of abstract interfaces for expanding to others, and the ability to pull various types of dependencies before a workflow starts. MaestroWF is actively developed and maintained at https://github.com/LLNL/maestrowf.

CG LIPID PHASE DETERMINATION. Our approach to phase determination involved two steps. First, we chose four simulations in which we visually classified the membrane phase as either gel (L_β), liquid ordered (L_o), liquid disordered (L_d), or a midpoint between L_o and L_d ($L_{d/o}$) (**Fig. S4A**). In making these selections, we required that the entire system was in a single phase, and contained both phospholipid species (although, out of necessity, the 100% DPPC system was used to represent the L_β phase). Second, we used these selected simulations to derive quantitative metrics for phase designation. To this end, we used the sampling from the last 1 μs of the bilayer's lower leaflet from each simulation to extract data from the lateral (in the plane of the membrane) cumulative radial distribution functions (cRDFs) of acyl chains around each lipid species – effectively measuring the average number of chains present in 0.02 nm radial bins around each lipid type. For this purpose, we used the C2A and C2B beads from DPPC, the D2A

and D2B beads from DOPC, and the R1 bead from cholesterol. From these cRDFs, we obtained phase-specific patterns of lipid-lipid packing. For example, the cRDF of the L_β phase has relatively high first and third peaks, combined with relatively low wells between the first, second, and third peaks (**Fig. S4B**). In practice, we used these cRDFs to define thresholds of specific peak heights and well depths that underlie our classification of lipid phase. As depicted in **Fig. S4B**, thresholds between the L_o and L_β phases were set to 10% beyond the extremes observed for the first and third peak height, and the first and second well depth. Thresholds between the L_o and L_d phases were set as halfway values (averaged for DPPC and DOPC) between the heights of the first, second, and third peaks for the $L_{d/o}$ and L_d profiles. cRDF profiles and associated phase classification thresholds were computed and applied separately for each set of parameters to ensure that the packing density was not sensitive to the different APLs reported in each model.

COMPARISON OF COMPUTED AND EXPERIMENTAL PHASE DIAGRAMS.

Classification was conducted separately for DOPC and DPPC to determine the overall phase behavior of the membrane, and whether different lipid types existed in the same phase or if there was phase coexistence. We apply this classification tool on a graded scale such that, depending on the specific shape of the cRDF for each lipid type, and how many of the thresholds were exceeded, we could qualify the probability of the L_d, L_o, or L_β phase being present in a system, on a scale from 0 to 1. Values from computation and experimental consensus average[63-66] phase behavior are indicated with superscript C and E, respectively. For example, the probability of the L_d phase being present in a simulated system is denoted as $P\left(\mathrm{L}_\mathrm{d}^\mathrm{C}\right)$. To compare simulation to

experiment at each point on the phase diagram, we computed the Euclidian distance, d, between these measures of lipid phase according to:

$$d = \sqrt{\left(P\left(\mathrm{L}_{\mathrm{d}}^{\mathrm{C}}\right) - P\left(\mathrm{L}_{\mathrm{d}}^{\mathrm{E}}\right)\right)^2 + \left(P\left(\mathrm{L}_{\mathrm{o}}^{\mathrm{C}}\right) - P\left(\mathrm{L}_{\mathrm{o}}^{\mathrm{E}}\right)\right)^2 + \left(P\left(\mathrm{L}_{\beta}^{\mathrm{C}}\right) - P\left(\mathrm{L}_{\beta}^{\mathrm{E}}\right)\right)^2}.$$

This evaluation is depicted graphically in **Fig. S5.** Finally, we computed the phase accuracy of each simulation as:

$$\text{phase accuracy} = \left(\sqrt{2} - d\right) \Big/ \sqrt{2} \times 100\%,$$

thus taking $d = \sqrt{2}$ to represent completely different phase behavior between computation and experiment.

VISUALIZATION AND ANALYSIS. Visualization of the lipid system, and illustration of lipid positions was implemented using VMD[67]. Locally written scripts, as well as GROMACS tools were used for the analysis. APL@Voro[68] was used to generate the Voronoi diagrams.

RESULTS

RE-PARAMETERIZATION OF DOPC AND DPPC LIPIDS

We refine CG Martini parameters for two commonly used model lipids (DOPC and DPPC) to improve their ability to replicate structural and thermodynamic properties and to enhance their ability to reproduce experimental temperature-dependent phase behavior in the ternary lipid mixture, DOPC/DPPC/CHOL. We ensure compatibility with the wide array of existing Martini parameters for other molecules by restricting our modifications to intra-molecular bond and angle terms of the force field. CG parameter refinement is carried out via a systematic iterative procedure to match bond length and angle distributions from CG simulations to those from AA simulations using the CHARMM36 force field (as described in the Methods).

The protocol for re-parameterization of CG parameters follow two parallel strategies to account for potential conflict with the Martini's building-block approach. When analyzing the distributions of the AA simulations, we observe that chemically similar headgroup regions of DPPC and DOPC can behave quantitatively differently even when in the same phase (**Figs. 1, S6 and S7**). A reasonably accurate re-parameterization, therefore, will need to deviate from the building-block approach. First, we re-parameterize the lipids under the constraint that parameters must be invariant among chemically identical regions in different lipids. Despite forfeiting some potential accuracy, these parameters retain Martini's generalized 'building block' philosophy. For this reason, these are termed the "Extensible parameters" (**Appendix 1**). Second, we adopt a

lipid-specific treatment to account for the qualitatively different behavior of DPPC and DOPC in AA simulations. This independent parameterization of DPPC and DOPC leads to lipid-specific parameters in some regions of shared chemical identity, such as lipid headgroup choline and glycerol moieties. While these "Optimal parameters" (**Appendix 2**) provide the most accurate fit to AA simulations, they suffer from a lack of modularity and, therefore, do not abide by the building block philosophy of Martini, which may in some cases be undesirable due to the increased parameterization burden. Details of re-parameterization are provided below under appropriate sections.

We profile the improvement attained by these re-parameterized lipids in terms of intra-molecular geometry distributions, structural and thermodynamic properties of pure bilayers, and phase diagram of the ternary lipid mixture. The lamellar phases formed by various DPPC/DOPC/CHOL combinations have been extensively characterized by experiment[8]. We use a consensus representation of this ternary phase diagram (**Figs. S8 and S9)** to evaluate the accuracy of parameters used in CG simulations of relatively large systems (~3,000 total lipids) conducted at 51 different compositions (**Fig. S3**). The emergence of lipid phases in these simulations is quantified based on patterns of species-specific radial packing (see Methods).

STANDARD MARTINI LIPID PARAMETERS (V2.2)

We begin by characterizing the currently available Martini model (V2.2) in terms of its reproducibility to sampled distributions of bond lengths and angles from AA simulations, and

how well it approaches the features observed in a ternary lipid phase diagram. These results are used as baseline to define the parameters that require improvement and as a reference for comparison to both of our improved "Extensible" and "Optimized" lipid parameters.

COMPARISON WITH ATOMISTIC INTRA-MOLECULAR GEOMETRY DISTRIBUTIONS. The full set of distance distributions between bonded CG beads and their analogous values sampled in AA simulations (after pseudo-CG mapping) for pure DPPC bilayer are shown in **Fig. S6.** In all cases, the peaks of the probability distributions for DPPC bond distances from standard Martini CG simulations (blue line) overlap with those of AA simulations (black lines). However, the CG distributions are, in general, broader than, and sometimes not properly aligned with those computed from AA simulations. In particular, the distributions of bond lengths between the choline-phosphate (connecting beads NC3 and PO4), and glycerol-glycerol (connecting beads GL1 and GL2) beads indicate that these groups are not drawn sufficiently close together (**Fig. 1C**). The angle distributions of DPPC sampled by the standard Martini V2.2 is generally better represented when compared with AA-derived simulations (**Fig. S7**). However, the exceptions are those angles measured between both the headgroup (NC3-PO4-GL1, blue line) and the glycerol moiety (GL1-GL2-C1B, blue line), which are too acute (**Fig. 1C**).

Concurrently, with the current Martini V2.2, DOPC distributions are particularly out of alignment with AA data corresponding to the oleoyl chains, where sampled bond distances are in general 1 Å too short (**Fig. S6**). Similar to the DPPC case, this behavior can be likely attributed to the fact that the standard Martini parameters for DOPC were derived from bulk alkenes

simulations. A point of attention is the evident deviation in the orientation of the choline group and the glycerol moiety, given by the pronounced divergence of their corresponding angle distributions (**Fig. 1D**).

STRUCTURAL AND THERMODYNAMIC PROPERTIES OF HOMOGENEOUS BILAYERS. To characterize structural profiles, we compute fluid phase electron density distributions for DPPC at 323 K and for DOPC at 310 K. Overall, the DPPC electron density profiles from AA simulations are well reproduced using the standard Martini CG parameters (**Fig. 2A**, dotted lines). Minor discrepancies include slight compaction of acyl-chains toward the bilayer center and overly rigidified choline placement slightly too far away from the bilayer center (**Fig. 2A**). The match between AA and CG profiles for DOPC (**Fig. 2A**) exhibits slightly lower fidelity than it does for DPPC. The largest deviation is found in the profile corresponding to the acyl-chain density, which is too high in the center of the bilayer (**Fig. 2B**).

The current Martini parameters generate fluid-phase area per lipid (APL) values that are consistently, slightly larger than the equivalent values from AA simulations (**Table 1**). Specifically, the CG APLs are ~ 0.02 and 0.01 nm^2 larger than the AA values for DPPC and DOPC, respectively. This small discrepancy is most likely due to higher flexibility of aliphatic tails in the CG model (see below), especially for the DPPC model.

To measure the internal structural ordering of the lipids, the second order parameter is calculated between every connected bead of the CG models. The equivalent bond order parameters are also measured using pseudo-CG positions extracted from the AA simulations. The internal structural ordering is qualitatively similar between the standard Martini and AA

simulations for both DPPC and DOPC (**Fig. 3A and B, respectively**). However, the lipid tails are systematically more disordered in the standard Martini simulations.

As reported in the original model[57], the current Martini V2.2 parameters underestimate the melting transition for DPPC, where the T_m is estimated to be 295 K[57], almost 20 K below the experimentally measured T_m of ~314 K[58].

PHASE DIAGRAM OF TERNARY LIPID MIXTURE. Consistent with previously published work[34, 44-45], the standard Martini V2.2 parameters for DPPC, DOPC, and CHOL do not phase separate at 298, or even 290 K in the physiologically relevant L_d/L_o coexistence region of the phase diagram (**Fig. 4A**). Indeed, only two systems in this region (21 and 39) show even moderate L_d/L_o heterogeneity (**Fig. S10)**. The degree of lateral heterogeneity in these systems is small compared to fully separating systems, and actually displays little difference in the properties of these regions. All other experimentally observed L_d/L_o separating compositions display no detectable separation of lipid species or properties. This general failure to adequately separate into L_d and L_o phases persists even when we reduce the simulation temperature to 290 K in an attempt to promote lipid de-mixing. Nevertheless, our extensive scanning of lipid compositions reveals that the standard Martini parameters accurately capture experimental phase behavior in many other regions of the ternary diagram, which we collectively quantify (see Methods) to be 63% correct (**Fig. 4A**). In particular, these parameters reproduce the single phase transition from L_d to L_o and the transition from L_β to L_o, in agreement with previous work[69-70]. Furthermore, several simulations in the bottom-right corner of the phase diagram (high DPPC, low DOPC, and low cholesterol concentration; systems 39, 43, 44, 47) that are close to the

experimental triple-phase coexistence region (**Figs. S8 and S9**) develop discrete pockets of L_β condensation (**Fig. S11**). To further test the robustness of the standard Martini V2.2 parameters, the complete phase diagram simulations are repeated at 310 K.

Given that little phase separation is observed at 290 K, it is not surprising that there is no phase separation at 310 K (**Fig. S12**). All L_β regions have disappeared at 310 K, and the boundary between L_d and L_o has shifted towards the upper right of the phase diagram. At least, these observations shifts are in line with what you might expect from the experimental findings.

EXTENSIBLE LIPID PARAMETERS

The Extensible parameters are generated using the 'building block' approach to simplify future optimization of additional lipids. As such, these Extensible parameters are designed to have transferable properties where common headgroups can be combined with different tails to generate new lipid species. To that end, despite the fact that the headgroup/linker regions in DPPC and DOPC AA simulations display slightly different bond length/angle distributions (**Figs. 1, S6, and S7**), the Extensible model is built to fit the combined, averaged distributions observed for these lipid headgroups.

RE-PARAMETERIZATION USING ATOMISTIC INTRA-MOLECULAR GEOMETRY DISTRIBUTIONS. The head group bond length distributions, specifically between choline-

phosphate, phosphate-glycerol, and glycerol-glycerol beads, are systematically too long in the current Martini V2.2 (**Figs. 1, S6**, blue lines). In order to alleviate the discrepancy, we first decrease the associated equilibrium bond distances for both DPPC and DOPC. Similarly, we focus on the angles involving both of the glycerol beads and the connecting bead to acyl-chain 2, for which angles sampled using the current Martini V2.2 are too acute (**Figs. 1, S7**, purple and blue lines). Consequently, the equilibrium angles for both GL1-GL2-C1B and GL2-GL1-C1A are optimized, again considering the averaging obtained from the corresponding AA distributions.

Most of the DPPC tail bond length distributions observed in Martini V2.2 are broader than observed in AA, leading us to increase the force constant for bonded terms from 1250 to 3500-3800 kJ mol^{-1} nm^{-2} for the tail beads. The force constant for angles between the tail particles are also increased from 25 to 35 kJ mol^{-1} rad^{-2}. These modifications yield CG parameters that more effectively capture the conformational distributions obtained in AA simulations (**Figs. 1, S6, and S7**).

Our approach to DOPC tail re-parameterization is conducted analogously to DPPC. After several iterations, we decided to re-map the oleoyl chains, starting from the proximal carbon to the glycerol moiety and mapping atomistic carbons to CG beads in a 4-5-4-5 pattern (alternating either 4 or 5 carbon atoms to each CG bead). Thus, each aliphatic chain is composed of 4 CG beads in total, where the double bond is localized between beads 2 and 3 (D2A and D2B) and represented using the C3 Martini bead type (alkene group). Overall, our Extensible model increases the equilibrium distances for all tail bonds and adjusts the force constant for the bonded terms to reflect the double or single bond chemistry. Similar to the results for DPPC, our

modifications to DOPC yield CG Martini parameters that improve the correlation between intramolecular configurations sampled in CG and AA representations (**Figs. 1, S6, and S7**).

STRUCTURAL AND THERMODYNAMIC PROPERTIES OF HOMOGENEOUS BILAYERS. The fluid phase electron density distributions for DPPC at 323 K and for DOPC at 310 K are again calculated. Overall, the Extensible parameters reproduce the DPPC electron density profiles from AA simulations (**Fig. 2A**, dashed lines). The same minor discrepancies are observed as with the standard Martini model, with a slightly rigid choline density. In contrast, CG parameter optimization for DOPC slightly increases membrane thickness, pushing choline and phosphate beads ~0.2 nm too far toward bulk water, though the acyl-chain density profile is in general improved (**Fig. 2A**, green dashed lines).

The APL for the DPPC and DOPC lipids, using the Extensible parameter set, displays an improved correlation to the AA values. DPPC now exhibits an average APL of 0.62 nm^2, which is only 0.01 nm^2 larger than AA value. The DOPC AA APL of 0.68 nm^2 is exactly reproduced by the Extensible CG parameters.

The internal structural ordering of DPPC, as measured by the second order parameter, displays slight, yet consistent improvement in AA agreement for almost all bonds when compared to the standard Martini. In particular, the acyl-chains display increased stiffness. In DOPC, there are some improvements in AA agreement seen in the head and backbone regions, while being qualitatively similar to the standard Martini in the acyl chains (**Fig 3B**).

The protocol described by Marrink *et al.*[57] can be used to estimate the T_m of DPPC in a homogenous lipid bilayer. In short, a CG bilayer containing both liquid and gel phases (**Fig. 5A**) is evolved at various temperatures, and the change in APL value is used as a metric for detecting which phase grows over time (gel phases having smaller APL values than liquid). Our Extensible Martini parameters favor gel phase up to temperatures of 305 K. On the other hand, an APL expansion is observed at 310K, suggesting a phase transition at such temperature (**Fig. 5B**, green line). This results in an estimate of 305 K $\leq T_m \leq$ 310 K for DPPC. While still below the experimental T_m ~314 K, this represents a 10 K improvement over the current Martini V2.2 value of 295 K.

PHASE DIAGRAM OF TERNARY LIPID MIXTURE. We proceed to evaluate the ability of the Extensible Martini parameters to reproduce the experimental phase diagram of DPPC/DOPC/CHOL at 298 K. The Extensible parameter simulations capture a large majority of the L_d/L_o coexistence (**Figs. 4B)**, and do so without the extension of this coexistence to other regions of the phase diagram, as it is seen with DPPC/DIPC/CHOL simulations (**Figs. S1 and S2**). Importantly, the phase coexistence behavior replicates experimental results in those lipid compositions that most closely match a chemical equilibrium in a cell membrane. Like standard Martini V2.2, our Extensible parameters reproduce the transition of the single fluid phase from L_d to L_o as the fraction of both DPPC and CHOL increases. Furthermore, all the possible combinations of coexisting lipid phases (L_o/L_d, L_d/L_β, L_o/L_β, and $L_d/L_o/L_\beta$) are replicated in the correct regions. Nevertheless, the region of L_d/L_β coexistence in the absence of cholesterol is still poorly resolved. Overall, the total phase accuracy of the Extensible parameters is calculated at just over 70%, demonstrating considerably increased accuracy compared to the Martini V2.2

parameters (63%). For lipid compositions within 20% of the critical point, a region mimicking physiological conditions, the Extensible parameters exhibit higher accuracy (77%) compared to the Martini V2.2 parameters (70%). Most of this improvement is achieved through replicating the L_o/L_d coexistence seen in the central section of the phase diagram.

When the phase diagram is repeated at 310 K (**Fig. S12**), we observe changes in phase coexistence patterning that is quintessentially representative of experimental findings: the region of phase coexistence shrinks, and the phase coexisting region shifts to compositions of higher DPPC/CHOL concentration. Given the sparse experimental data for phase diagrams at higher temperatures, we cannot quantitatively compare the 310K phase diagram against experiment data, as was done for the 298 K phase diagram.

OPTIMAL LIPID PARAMETERS

In contrast to the Extensible parameters, where headgroup bond length/angle distributions over the DPPC and DOPC AA simulations were combined to model an 'average' phosphatidylcholine headgroup, the Optimal parameters are fit purely to the distributions observed in each respective lipid using CHARMM36. As such, the slight differences in the bond/angles distributions are independently captured, so the lipid-dependent behavior manifested in the AA simulations is explicitly replicated in the Optimal parameter model.

RE-PARAMETERIZATION USING ATOMISTIC INTRA-MOLECULAR GEOMETRY DISTRIBUTIONS. Similarly to the Extensible parameters, the force constant for bonded terms is increased from 1250 to ~2000 kJ mol^{-1} nm^{-2} for particles connecting the choline and glycerol beads. The exception is the bond connecting the phosphate (PO4) and the first glycerol (GL1), for which force constant was raised to 9000 kJ mol^{-1} nm^{-2}. Clearly, this suggests a stiffness of this particular region, modulating compaction of the head group. Similarly, associated angle equilibrium values were set to smaller values (**Fig. 1, S7**, red lines) in comparison with the standard Martini (blue lines) to better agree with the distributions obtained from CHARMM36.

The Optimal DOPC bond parameters are similar to the Extensible parameters in terms of bead-mapping and general trends of bond length and stiffness. The lipid-specific headgroup angles are reproduced from the AA distributions, especially the angle involving the headgroup choline bead, which is particularly poorly fit in standard Martini V2.2 (**Fig. S7)**. In contrast to the DPPC parameters, the force constant involving GL1-GL2-C1B and GL2-GL1-C1A angles is actually decreased.

The force constant of the connecting bonds in the DPPC acyl chains are raised by ~2000 kJ mol^{-1} nm^{-2}, while equilibrium distances are retained from the standard Martini model. Regarding angles, the force constant is increased even further compared to the Extensible parameters. Overall, these changes increase the lipid's stiffness which, combined with the increased bond forces, improves the accuracy of DPPC's T_m (see next section). As expected, due to the specific fitting to the DPPC AA simulations, the bond and angle terms (particularly in the headgroups and linker regions) produce Martini parameters that more precisely capture the conformational distributions obtained at AA resolution (**Figs. 1, S6, and S7**).

For DOPC acyl chains, bond distances were set to 0.55 nm to account for the length differences when compared to the aliphatic tails in DPPC (**Fig. S6**, red lines). Angles connecting the beads within the saturation region are set at values similar to the ones obtained for DPPC. However, the kink associated by the presence of the double bonds required an equilibrium angle set to 130 degrees. This modification provides a further pronounced difference between the two lipid types and an inherent flexibility of DOPC, which is challenging to achieve using a building block approach.

STRUCTURAL AND THERMODYNAMIC PROPERTIES OF HOMOGENEOUS BILAYERS. The electron density distributions for both DPPC and DOPC in the fluid phase are extremely similar to the Extensible parameters, whereby the DPPC profile matches AA simulations very closely, and the DOPC profile displays a slight displacement of the headgroup beads (**Fig. 2B dashed lines**). The APLs observed for both the DPPC and DOPC lipids, using the Optimized CG parameters, are an exact match for what is calculated from the AA simulations (0.61 nm^2 for DPPC and 0.68 nm^2 for DOPC), a slight improvement over both the Extensible parameters and standard Martini (**Table 1**).

The internal structural ordering of the Optimized CG parameters exhibits moderately better agreement with data from AA simulations for both DPPC and DOPC (**Figs. 3A and 3B**). In particular, the further increased order in DPPC acyl-chains, introduced by stiffer bond and angle terms in our Optimized CG parameters, yields good improvement in a region that is systematically too disordered in standard Martini simulations (**Fig. 3A**). However, our parameter modifications do not fix an analogous bias toward acyl-chain disorder for DOPC (**Fig. 3B**).

In addition, we have computed a related mechanical property for pure DPPC bilayers. The compressibility moduli (K_a) for a DPPC bilayer in the liquid phase (278 ± 14 mN/m) is in good agreement with a value reported previously for the original Martini lipid model, and slightly higher than experimental values (260 mN/m, at 315 K)[71]. Likewise, the K_a for the gel phase at 297 K (1645 ± 24 mN/m) is almost identical to the experimental value of 1650 mN/m (at 300 K)[71].

With the Optimal parameters, an overall improved melting temperature is obtained for a pure DPPC bilayer. As shown in **Fig. 5C**, the set of Optimal Martini parameters provides a clear estimation of 313 K ≤ T_m ≤ 315 K for DPPC, which is in excellent agreement with experiments[58, 72]. As expected from the parameterization consistency, this value also agrees with the estimates obtained from the AA simulations (315 K ≤ T_m ≤ 317.5 K; **Fig. S13 and Supporting Results**). The same T_m calculation protocol was repeated using a range of hydration levels (a range of 5-30 waters per lipid). The T_m is only affected once the hydration level is very low, ≤ 10 waters per lipid (**Fig. S14A**), in alignment with previous calculations[57].

Close inspection of the simulated systems near the T_m (310-315 K) reveals the presence of membrane deformations; which are unable to fully destabilize the gel phase. Previous observation of such deformations using the Martini force field has been attributed to the formation of ripple phases[73]. Surprisingly, spontaneous lipid tilting is also observed in the gel phase (**Fig. S14B and C**), otherwise obtained only using enhanced sampling techniques[74].

The Optimal DPPC lipid parameters also show improved correlation with AA simulations at higher temperatures (**Fig. S15 and S16**). APL values (**Fig. S15**), as well as lipid tail order

parameters (**Fig. S16**) from the AA simulations are much better matched by the Optimal CG parameters than the standard Martini (V2.2). Overall, this set of results suggests that the parameters could be potentially used in conditions other than those used for the initial parameterization.

PHASE DIAGRAM OF TERNARY LIPID MIXTURE. We next evaluate the ability of the Optimal parameters to reproduce the experimental phase diagram of DPPC/DOPC/CHOL at 298 K. As with the Extensible parameters, they capture the L_d/L_o coexistence region in the physiologically relevant region of the phase diagram without inaccurate extension of this coexistence to other regions (**Fig. 4C**). This L_d/L_o coexistence region achieves better representation of the experimental consensus than produced by the Extensible parameters. Furthermore, the $L_d/L_o/L_\beta$ cholesterol-containing triple phase region is also much more accurately represented in the Optimal parameters.

Importantly, the Optimal parameters exhibit some L_d/L_β phase separation in a binary mixture of DPPC and DOPC (**Fig. 4C**), which is indicated by experiment (**Figs. S8 and S9**) but does not emerge with standard Martini or even our Extensible parameters (**Figs. 4A and B**). Specifically, system 50 (90% DPPC, 10% DOPC, no cholesterol) undergoes extensive de-mixing with the Optimal parameters, but not with standard Martini parameters for DPPC mixed with either DOPC or DIPC (**Fig. S17**). The total phase accuracy of the optimal parameters is 76%, an improvement from the Extensible parameters (70%) and an even more pronounced increase in accuracy over the standard Martini V2.2 parameters (63%). Significant improvement is seen in compositions within 20% of critical point, where the optimal parameters provide a phase accuracy of 84% compared to 70% from the standard Martini. Nevertheless, the optimal

parameters still fail to fully sample robust L_d/L_β coexistence in the absence of cholesterol when global DPPC content falls below 90%.

Again, when the temperature is increased to 310 K, the phase diagram qualitatively displays the same tendencies as the Extensible parameters, and trends follow experimental observations. However, the degree to which the L_d/L_o coexistence region decreases appears to be quantitatively less than is observed for the Extensible parameters, and as a consequence of the higher T_m for DPPC in the Optimal parameters.

DISCUSSION AND CONCLUSIONS

The Martini force field has gained extensive applicability by striking the right balance between universality and accuracy. Here, we have refined the Martini CG parameters for DPPC and DOPC to improve their phase behavior using both Extensible ("building-block") and Optimized ("lipid-specific") approaches. When compared to the standard Martini parameters, these refinements show only minor effects on the lipid density profiles (**Fig. 2**) and APL values (**Table 1**) of DPPC and DOPC, while providing moderate improvement for several DPPC order parameters (**Fig. 3A**). In the Extensible and Optimal parameter sets, we made the modifications to lipid topologies with the goal of improving the phase-segregation behavior for DPPC/DOPC/CHOL mixture, something which it not attainable using the standard Martini. Each lipid species is parameterized using homogenous AA simulations at a single temperature. Regardless of this, the lipid parameters show transferability potential given that they can mix with each other, and the current Martini cholesterol model, as well as temperature dependence both below and above their parameterization conditions.

One of the reasons that the refined parameter sets are able to properly capture phase separation is due to improved melting transition temperatures of lipids. The prevalence of experimental T_m measurements for the system studied here and the accepted existence of such phase transitions makes this a useful comparison through which the potential limitations in CG models can be identified. The re-parameterization of CG bonded terms, only required fitting to the intramolecular geometrical distributions obtained from atomistic simulations. In standard Martini, these distributions were parameterized based on the dynamics of alkane chains in bulk

systems and were not laterally restricted and consequently lack the inherent order and packing of the lamellar state. Thus, as done here, reparameterization of the potentials of aliphatic tails in the Extensible and Optimal parameter sets greatly improves T_m estimates. This approach can be easily extended to other high melting lipids like sphyngosines, ceramides, and cerebrosides.

In addition, the re-parameterization increases the line tension between DPPC and DOPC in the presence of cholesterol, leading to proper L_o/L_d phase separation. This remarkable achievement opens the possibility to use more biologically-relevant lipids in combination with other biomolecules. Importantly, when considering regions of the phase diagram encompassing lipid concentrations, mimicking physiological conditions (within 20% of critical point), The Optimal parameter set yields a phase accuracy of 84% compared to 70% accuracy obtained with the standard Martini V2.2 and 68% accuracy for the DPPC/DIPC/CHOL system (see SI). Besides the lack of experimental accuracy within this region, our results suggest that the optimized set is able to discriminate subtle changes in lipid composition, which may lead to phase-demixing. This behavior enables fine-tuning of the lipid component fractions to allow for fluctuating domains to form, much like the phenomena that can occur within *in vitro* systems, and provides a more accurate environment for studying the structure and dynamics of membranes and embedded proteins. These fluctuating domains do not occur with any of the DPPC/DOPC/CHOL or DPPC/DIPC/CHOL compositions using the standard Martini V2.2.

The Extensible and Optimal parameter sets capture the temperature dependence of relative mobility of individual lipids leading to improved phase behavior of the lipid bilayer. Experimentally, the general consensus on the effect of temperature on the phase diagram is that as temperature increases, the L_β phases begin to disappear and the region of L_o/L_d coexistence shrinks towards the direction of increased DPPC and CHOL percentage[64]. However, the precise

degree to which the coexistence region depletes and the measured temperature at which phase coexistence disappears is found to vary[63, 75-76]. Nevertheless, the refined Martini parameters very closely reproduce these experimental observations.

We note that the deficiency in L_d/L_o coexistence in the absence of cholesterol is the only qualitative inconsistency between experiments and the results of simulations with the Optimized parameters, whose collective accuracy is 76%. Several of the compositions that are inaccurately represented by the Optimized parameters display significant experimental variability[63-66] (for example composition 30/30/40 is only identified as phase separating in 50% of the experimental results) and that our quantification of phase accuracy incorporates additional details regarding precisely which phases and phase mixtures are present. Given that we employ a consensus of several experimental studies, some simulations may be penalized for not exactly containing the same mixture of phases. The average phase accuracy of each of the single experimental phase diagrams compared to the consensus is ~82%. Thus, there exists a certain degree of uncertainty between different experimental measurements and techniques that needs to be accounted for when comparisons are made with the simulated phase diagram.

In summary, our study provides a strategy to further refine the lipid parameters of the Martini force field by fitting the bonded terms to the intramolecular degrees of freedom obtained from atomistic simulations. This approach leads to improvements in both the melting temperature and the lipid phase separation. The resulting lipid parameters accurately reproduce the experimentally measured complete phase diagram for the DPPC/DOPC/CHOL ternary lipid mixture, which was not previously achieved with the standard Martini lipid force field. In compositions within ~10% of the critical point, our Optimized Parameters yield a 30% improvement in accuracy over the standard Martini lipid parameters, correctly reproducing 92%

of the correct phases. These studies indicate that our parameters show improved properties that have been rigorously examined in the lamellar bilayer structure. Importantly, with the proposed parameterization protocol, such improvements are preserved for other membrane structures, such as the inverted hexagonal phase and a vesicle **(Figs. S18 and S19)**.

Furthermore, this study highlights two powerful aspects of the Martini force field. First, there is a great potential to improve the lipid phase behavior within the already defined building block framework of Martini while maintaining the chemical invariability of beads. Accordingly, the Extensible parameter set achieves the right balance between accuracy and portability for situations where there is a need to consider a mixture comprising hundreds of lipids for mimicking the plasma membrane. Second, Martini can serve as the initial framework to derive a highly optimal CG lipid parameter set that can quantitatively reproduce all-atom MD and/or experimental results. As shown here, the Optimal parameter set obtained by relaxing the building-block modularity allows one to capture accurate lipid phase behavior at high precision. The improvement provided by the refined lipid parameter sets could be of great value to understanding lipid behavior within phase regions.

FIGURES

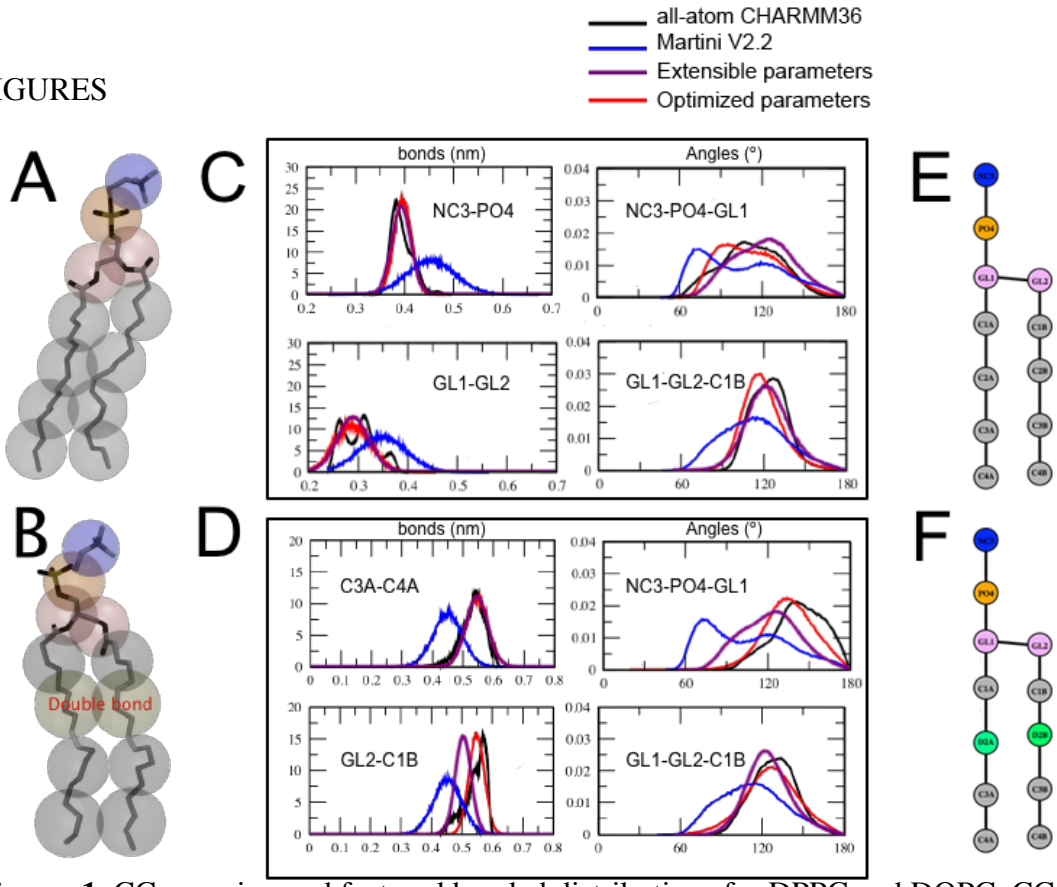

Figure. 1. CG mapping and featured bonded distributions for DPPC and DOPC. CG bead mapping for DOPC (A) and DPPC (B) lipids. Bead colors represent the different chemical groups as in the original Martini parameters set and mapped on all-atom backbone shown as a stick diagram. Hydrogens in the atomistic representations are not depicted for clarity. The unsaturation in the aliphatic tails is highlighted. Color code: blue beads: choline groups, orange beads: phosphates, pink beads: glycerols, gray beads: acyl chains, tan beads: double bond in DOPC. Representative intramolecular geometrical distributions are provided for DOPC (C) and DPPC (D) standard Martini along with all-atom distributions that were used for re-paramterization. Also, shown are the resulting reparameterized distributions for Extensible and Optimal parameter sets. The full sets of distributions as well as the numbering reference are provided in Supportive Figs. S6 and S7. The CG bead types associated with these bond and angle distributions are schematically shown for DOPC (E) and DPPC (F).

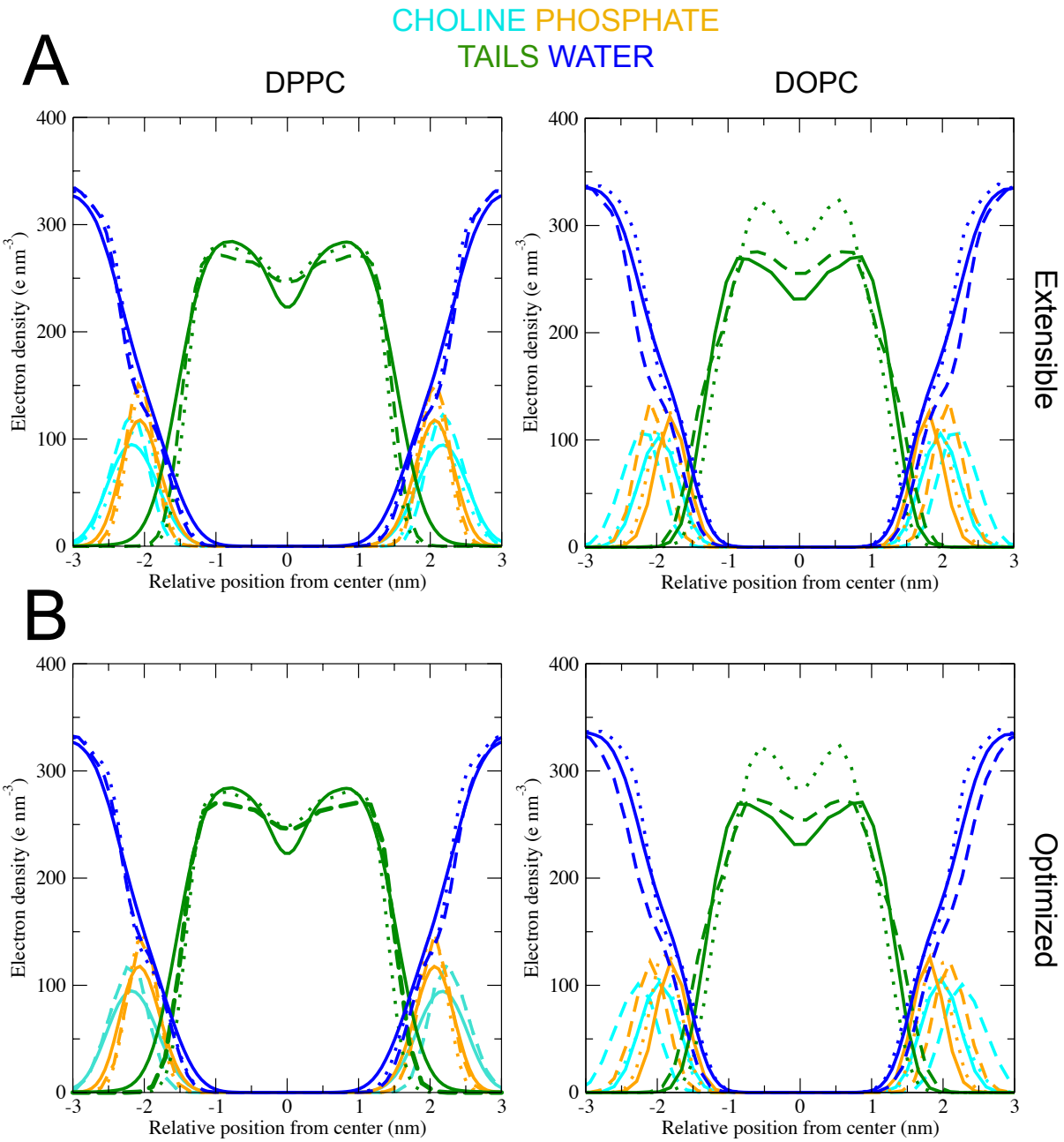

Figure. 2. Electron densities of DPPC and DOPC membranes in liquid state. (A) Profiles for the re-parameterized Extensible set (dotted lines) are compared with atomistic CHARMM36 (solid lines) and the standard Martini V2.2 (dashed lines). (B) Profiles for the re-parameterized Optimized set (dotted lines) are compared with atomistic CHARMM36 (solid lines) and the standard Martini V2.2 (dashed lines). Densities were computed by dividing the box in 100 slices and across the Z normal of the membranes.

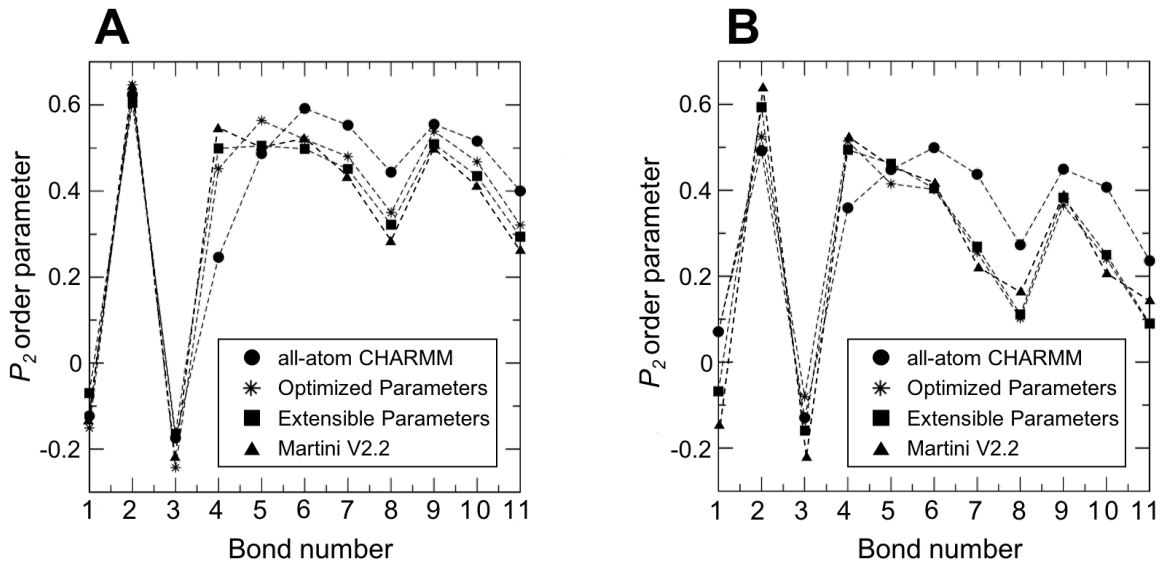

Figure. 3. Computed P_2 order parameters for DPPC and DOPC. P_2 parameters for CHARMM36 were computed after mapping the trajectory into a pseudo CG-representation. (A) P_2 computed for DPPC. (B) P_2 values computed for DOPC.

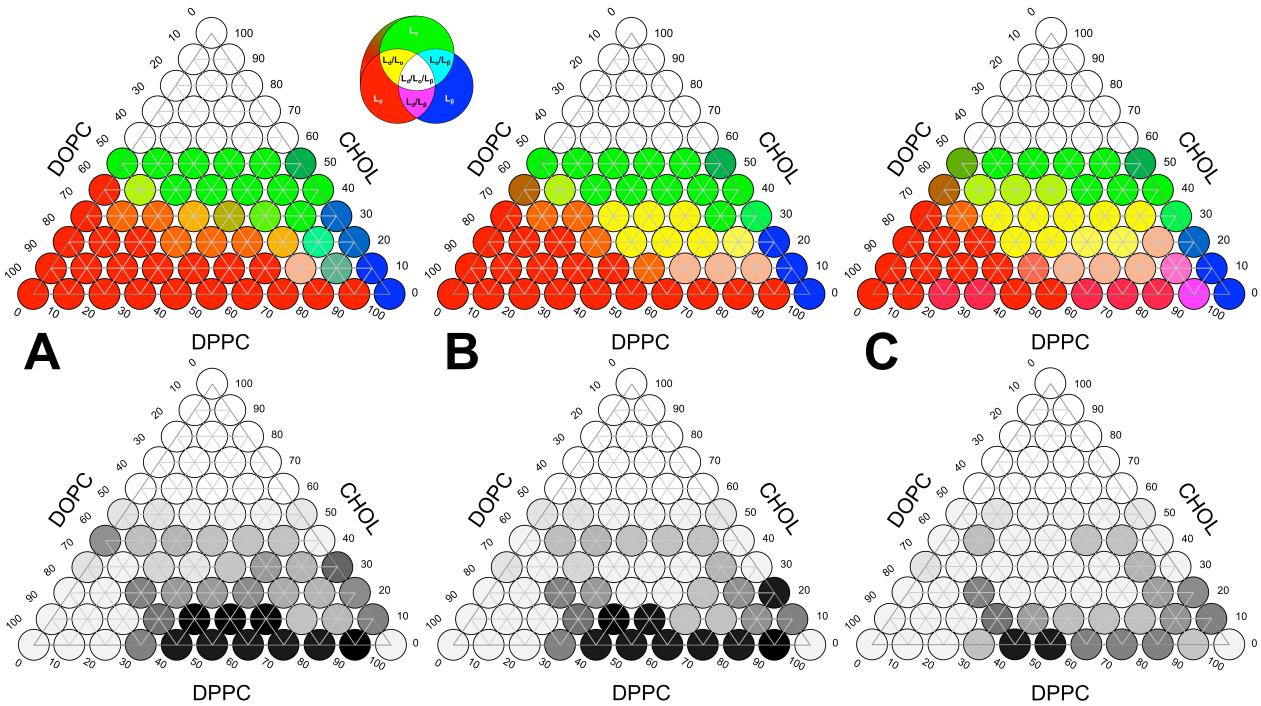

Figure. 4. The phase diagrams for the DPPC/DOPC/CHOL lipid mixtures. The complete phase diagram simulations as performed with the current Martini V2.2 (A), Extensible parameter set (B), and Optimal parameter set (C) are shown. The color scale for the upper images are shown in the inset color-combination key, where the three phase (L_d/L_o/L_β) are colored red, green, and blue, respectively, and combinations of those colors indicate which phases are present in the simulation (For further details, see **Fig. S5 and S9**). The lower images show the same phase diagrams colored on a black to white color scale to indicate the experimental accuracy of the simulation, where white is an accurate replication of the experimental data (For further details, see **Fig. S4, S5, and S9**).

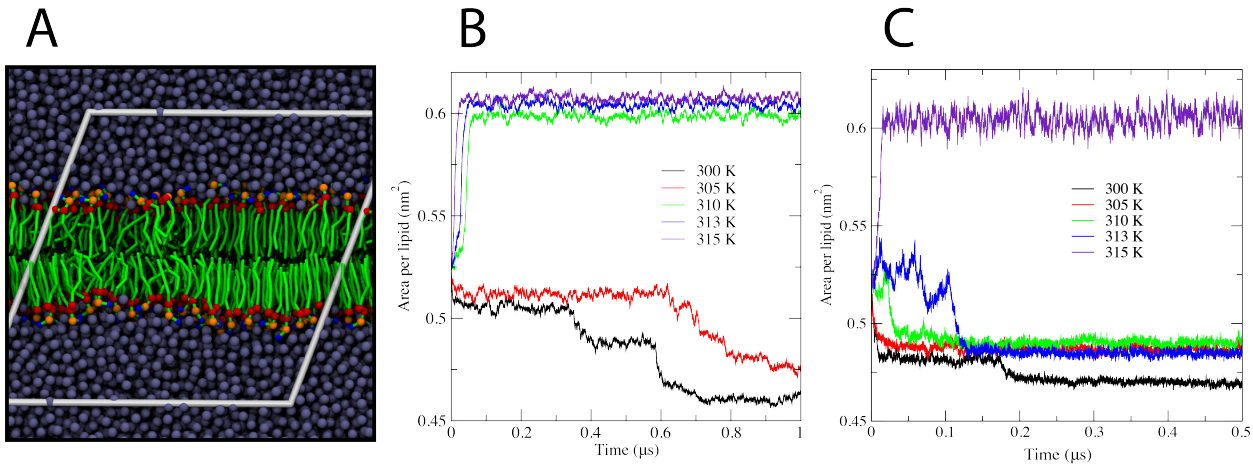

Figure. 5. T_m calculation for DPPC. (A) Initial coexisting L_d/L_β system box for computing T_m (see methods). (B) Area per lipid evolution at different temperatures for the Extensible model. (C) Area per lipid evolution at different temperatures for the Optimized model. The latter reproduces the experimental observed value (314 K). Image A shows a Martini simulation snapshot where the lipid tails are illustrated in green, the glycerol backbone beads are red spheres, the phosphate bead is orange, and the choline bead is blue. Water is shown as violet spheres.

TABLES.

Table 1. Area per lipid (APL) comparisons.

Lipid	Temp. (K)	APL (nm^2)			
		AA	Standard CG	Extensible CG	Optimized CG
DPPC	323	0.61±0.002	0.63±0.006	0.62±0.003	0.61±0.008
	290/298	0.49±0.001	0.47±0.0001	0.47±0.0007	0.47±0.0001
DOPC	310	0.68±0.012	0.69±0.007	0.68±0.003	0.68±0.012

Each equilibrated region of the trajectory was segmented in three equally independent blocks and the standard error was obtained.

ASSOCIATED CONTENT

Supporting Information.

The following files are available free of charge on the ACS Publications website at DOI: xxxx.

Appendix 1 (word document). The 'Extensible parameters' for both DPPC and DOPC.

Appendix 2 (word document). The 'Optimal parameters' for both DPPC and DOPC.

Supplementary Information (PDF). Supplementary methods and results; AA simulations for CG re-parameterization, biased generation of AA gel phases, DPPC melting temperature in AA simulations, CG lipid phase separation, second order parameter (P_2) and radial distribution functions (g(r)) for DPPC and DOPC, Martini V2.2 DPPC/DIPC/CHOL simulations and phase diagrams. Supporting figures; Fig.S1 to Fig.S20.

AUTHOR INFORMATION

Corresponding Author

*To whom correspondence should be addressed:

Felice C. Lightstone, Biosciences and Biotechnology Division, Physical and Life Sciences Directorate, Lawrence Livermore National Laboratory (LLNL), Livermore, California, 94550, USA; Tel: +1-925-423-8657, Fax: +1-925-423-0785, e-mail: lightstone1@llnl.gov.

S. Gnanakaran, Theoretical Biology and Biophysics Group, Los Alamos National Laboratory (LANL), Los Alamos, New Mexico, 94550, USA; Tel: +1-505-665-1923, Fax: +1-505-665-3493, e-mail: gnana@lanl.gov.

Present Addresses

†Current address: Syneos Health, Clinical division, Princeton, New Jersey, USA.

Author Contributions

The manuscript was written through contributions of all authors. All authors have given approval to the final version of the manuscript. ‡T.S.C. and C.A.L contributed equally.

ACKNOWLEDGMENT

This work has been supported in part by the Joint Design of Advanced Computing Solutions for Cancer (JDACS4C) program established by the U.S. Department of Energy (DOE) and the National Cancer Institute (NCI) of the National Institutes of Health. We thank the Livermore Institutional Grand Challenge and LANL Institutional computing for the computing time.

This work was performed under the auspices of the U.S. Department of Energy by Lawrence Livermore National Laboratory under Contract DE-AC52-07NA27344, Los Alamos National Laboratory under Contract DE-AC5206NA25396, Oak Ridge National Laboratory under Contract DE-AC05-00OR22725, and Frederick National Laboratory for Cancer Research under Contract HHSN261200800001E. C.N. is supported by U.S. Department of Energy LDRD funds. LLNL-JRNL-750994. LAUR:18-23792.

ABBREVIATIONS

AA, all-atom; APL, area per lipid; CG, coarse-grained; LJ, Lennard-Jones; L_d, liquid-disordered phase; L_o, liquid-ordered phase; RDF, radial distribution function.

REFERENCES

1. Elson, E. L.; Fried, E.; Dolbow, J. E.; Genin, G. M., Phase separation in biological membranes: integration of theory and experiment. *Annu Rev Biophys* **2010,** *39*, 207-226.

2. Lindner, R.; Knorr, R., Rafting trips into the cell. *Commun Integr Biol* **2009,** *2*, 420-421.

3. Lingwood, D.; Simons, K., Lipid rafts as a membrane-organizing principle. *Science* **2010,** *327*, 46-50.

4. Sezgin, E.; Levental, I.; Mayor, S.; Eggeling, C., The mystery of membrane organization: composition, regulation and roles of lipid rafts. *Nat Rev Mol Cell Biol* **2017,** *18*, 361-374.

5. Nyholm, T. K., Lipid-protein interplay and lateral organization in biomembranes. *Chem Phys Lipids* **2015,** *189*, 48-55.

6. Levental, I.; Veatch, S., The Continuing Mystery of Lipid Rafts. *J Mol Biol* **2016,** *428*, 4749-4764.

7. Wang, C.; Yu, Y.; Regen, S. L., Lipid Raft Formation: Key Role of Polyunsaturated Phospholipids. *Angew Chem Int Ed Engl* **2017,** *56*, 1639-1642.

8. Marsh, D., Liquid-ordered phases induced by cholesterol: a compendium of binary phase diagrams. *Biochim Biophys Acta* **2010,** *1798*, 688-699.

9. Koynova, R.; Caffrey, M., An index of lipid phase diagrams. *Chem Phys Lipids* **2002,** *115*, 107-219.

10. Curthoys, N. M.; Parent, M.; Mlodzianoski, M.; Nelson, A. J.; Lilieholm, J.; Butler, M. B.; Valles, M.; Hess, S. T., Dances with Membranes: Breakthroughs from Super-resolution Imaging. *Curr Top Membr* **2015,** *75*, 59-123.

11. Kotani, N.; Nakano, T.; Ida, Y.; Ito, R.; Hashizume, M.; Yamaguchi, A.; Seo, M.; Araki, T.; Hojo, Y.; Honke, K.; Murakoshi, T., Analysis of lipid raft molecules in the living brain slices. *Neurochem Int* **2017**.

12. Ceccarelli, A.; Di Venere, A.; Nicolai, E.; De Luca, A.; Rosato, N.; Gratton, E.; Mei, G.; Caccuri, A. M., New insight into the interaction of TRAF2 C-terminal domain with lipid raft microdomains. *Biochim Biophys Acta* **2017,** *1862*, 813-822.

13. Kabouridis, P. S., Lipid rafts in T cell receptor signalling. *Mol Membr Biol* **2006,** *23*, 49-57.

14. Villar, V. A.; Cuevas, S.; Zheng, X.; Jose, P. A., Localization and signaling of GPCRs in lipid rafts. *Methods Cell Biol* **2016,** *132*, 3-23.

15. Lorent, J. H.; Diaz-Rohrer, B.; Lin, X.; Spring, K.; Gorfe, A. A.; Levental, K. R.; Levental, I., Structural determinants and functional consequences of protein affinity for membrane rafts. *Nat Commun* **2017,** *8*, 1219.

16. Frewein, M.; Kollmitzer, B.; Heftberger, P.; Pabst, G., Lateral pressure-mediated protein partitioning into liquid-ordered/liquid-disordered domains. *Soft Matter* **2016,** *12*, 3189-3195.

17. Li, L.; Hu, J.; Shi, X.; Shao, Y.; Song, F., Lipid rafts enhance the binding constant of membrane-anchored receptors and ligands. *Soft Matter* **2017,** *13*, 4294-4304.

18. Eggeling, C.; Ringemann, C.; Medda, R.; Schwarzmann, G.; Sandhoff, K.; Polyakova, S.; Belov, V. N.; Hein, B.; von Middendorff, C.; Schonle, A.; Hell, S. W., Direct observation of the nanoscale dynamics of membrane lipids in a living cell. *Nature* **2009,** *457*, 1159-1162.

19. Mayor, S.; Rao, M., Rafts: scale-dependent, active lipid organization at the cell surface. *Traffic* **2004,** *5*, 231-240.

20. Rayermann, S. P.; Rayermann, G. E.; Cornell, C. E.; Merz, A. J.; Keller, S. L., Hallmarks of Reversible Separation of Living, Unperturbed Cell Membranes into Two Liquid Phases. *Biophys J* **2017,** *113*, 2425-2432.

21. Pusterla, J. M.; Schneck, E.; Funari, S. S.; Deme, B.; Tanaka, M.; Oliveira, R. G., Correction: Cooling induces phase separation in membranes derived from isolated CNS myelin. *PLoS One* **2017,** *12*, e0189142.

22. Schmidt, C.; Kim, D.; Ippolito, G. C.; Naqvi, H. R.; Probst, L.; Mathur, S.; Rosas-Acosta, G.; Wilson, V. G.; Oldham, A. L.; Poenie, M.; Webb, C. F.; Tucker, P. W., Signalling of the BCR is regulated by a lipid rafts-localised transcription factor, Bright. *EMBO J* **2009,** *28*, 711-724.

23. Mielenz, D.; Vettermann, C.; Hampel, M.; Lang, C.; Avramidou, A.; Karas, M.; Jack, H. M., Lipid rafts associate with intracellular B cell receptors and exhibit a B cell stage-specific protein composition. *J Immunol* **2005,** *174*, 3508-3517.

24. Bagam, P.; Singh, D. P.; Inda, M. E.; Batra, S., Unraveling the role of membrane microdomains during microbial infections. *Cell Biol Toxicol* **2017,** *33*, 429-455.

25. Johannes, L., Shiga Toxin-A Model for Glycolipid-Dependent and Lectin-Driven Endocytosis. *Toxins (Basel)* **2017,** *9*.

26. Morante, K.; Caaveiro, J. M.; Tanaka, K.; Gonzalez-Manas, J. M.; Tsumoto, K., A pore-forming toxin requires a specific residue for its activity in membranes with particular physicochemical properties. *J Biol Chem* **2015,** *290*, 10850-10861.

27. Sevcsik, E.; Schutz, G. J., With or without rafts? Alternative views on cell membranes. *Bioessays* **2016,** *38*, 129-139.

28. Rosetti, C. M.; Mangiarotti, A.; Wilke, N., Sizes of lipid domains: What do we know from artificial lipid membranes? What are the possible shared features with membrane rafts in cells? *Biochim Biophys Acta* **2017,** *1859*, 789-802.

29. Sodt, A. J.; Sandar, M. L.; Gawrisch, K.; Pastor, R. W.; Lyman, E., The molecular structure of the liquid-ordered phase of lipid bilayers. *J Am Chem Soc* **2014,** *136*, 725-732.

30. Sodt, A. J.; Pastor, R. W.; Lyman, E., Hexagonal Substructure and Hydrogen Bonding in Liquid-Ordered Phases Containing Palmitoyl Sphingomyelin. *Biophys J* **2015,** *109*, 948-955.

31. Marrink, S. J.; Risselada, H. J.; Yefimov, S.; Tieleman, D. P.; de Vries, A. H., The MARTINI force field: coarse grained model for biomolecular simulations. *J Phys Chem B* **2007,** *111*, 7812-7824.

32. Marrink, S. J.; Tieleman, D. P., Perspective on the Martini model. *Chem Soc Rev* **2013,** *42*, 6801-6822.

33. Risselada, H. J.; Marrink, S. J., The molecular face of lipid rafts in model membranes. *Proc Natl Acad Sci U S A* **2008,** *105*, 17367-17372.

34. Domanski, J.; Marrink, S. J.; Schafer, L. V., Transmembrane helices can induce domain formation in crowded model membranes. *Biochim Biophys Acta* **2012,** *1818*, 984-994.

35. Schafer, L. V.; de Jong, D. H.; Holt, A.; Rzepiela, A. J.; de Vries, A. H.; Poolman, B.; Killian, J. A.; Marrink, S. J., Lipid packing drives the segregation of transmembrane helices into disordered lipid domains in model membranes. *Proc Natl Acad Sci U S A* **2011,** *108*, 1343-1348.

36. Klingelhoefer, J. W.; Carpenter, T.; Sansom, M. S., Peptide nanopores and lipid bilayers: interactions by coarse-grained molecular-dynamics simulations. *Biophys J* **2009,** *96*, 3519-3528.

37. Ingolfsson, H. I.; Melo, M. N.; van Eerden, F. J.; Arnarez, C.; Lopez, C. A.; Wassenaar, T. A.; Periole, X.; de Vries, A. H.; Tieleman, D. P.; Marrink, S. J., Lipid organization of the plasma membrane. *J Am Chem Soc* **2014,** *136*, 14554-14559.

38. Ingolfsson, H. I.; Carpenter, T. S.; Bhatia, H.; Bremer, P. T.; Marrink, S. J.; Lightstone, F. C., Computational Lipidomics of the Neuronal Plasma Membrane. *Biophys J* **2017,** *113*, 2271-2280.

39. Marrink, S. J.; de Vries, A. H.; Mark, A. E., Coarse Grained Model for Semiquantitative Lipid Simulations. *The Journal of Physical Chemistry B* **2004,** *108*, 750-760.

40. Lopez, C. A.; Sovova, Z.; van Eerden, F. J.; de Vries, A. H.; Marrink, S. J., Martini Force Field Parameters for Glycolipids. *J Chem Theory Comput* **2013,** *9*, 1694-1708.

41. Wassenaar, T. A.; Ingolfsson, H. I.; Bockmann, R. A.; Tieleman, D. P.; Marrink, S. J., Computational Lipidomics with insane: A Versatile Tool for Generating Custom Membranes for Molecular Simulations. *J Chem Theory Comput* **2015,** *11*, 2144-2155.

42. Khelashvili, G.; Kollmitzer, B.; Heftberger, P.; Pabst, G.; Harries, D., Calculating the Bending Modulus for Multicomponent Lipid Membranes in Different Thermodynamic Phases. *J Chem Theory Comput* **2013,** *9*, 3866-3871.

43. Hakobyan, D.; Heuer, A., Phase separation in a lipid/cholesterol system: comparison of coarse-grained and united-atom simulations. *J Phys Chem B* **2013,** *117*, 3841-3851.

44. Davis, R. S.; Sunil Kumar, P. B.; Sperotto, M. M.; Laradji, M., Predictions of phase separation in three-component lipid membranes by the MARTINI force field. *J Phys Chem B* **2013,** *117*, 4072-4080.

45. Baoukina, S.; Mendez-Villuendas, E.; Tieleman, D. P., Molecular view of phase coexistence in lipid monolayers. *J Am Chem Soc* **2012,** *134*, 17543-17553.

46. Baoukina, S.; Rozmanov, D.; Tieleman, D. P., Composition Fluctuations in Lipid Bilayers. *Biophys J* **2017,** *113*, 2750-2761.

47. Hakobyan, D.; Heuer, A., Key molecular requirements for raft formation in lipid/cholesterol membranes. *PLoS One* **2014,** *9*, e87369.

48. Klauda, J. B.; Venable, R. M.; Freites, J. A.; O'Connor, J. W.; Tobias, D. J.; Mondragon-Ramirez, C.; Vorobyov, I.; MacKerell, A. D., Jr.; Pastor, R. W., Update of the CHARMM all-atom additive force field for lipids: validation on six lipid types. *J Phys Chem B* **2010,** *114*, 7830-7843.

49. Bjelkmar, P.; Larsson, P.; Cuendet, M. A.; Hess, B.; Lindahl, E., Implementation of the CHARMM force field in GROMACS: analysis of protein stability effects from correction maps, virtual interaction sites, and water models. *J. Chem. Theory Comput.* **2010,** *6*, 459-466.

50. Wassenaar, T. A.; Pluhackova, K.; Bockmann, R. A.; Marrink, S. J.; Tieleman, D. P., Going Backward: A Flexible Geometric Approach to Reverse Transformation from Coarse Grained to Atomistic Models. *J Chem Theory Comput* **2014,** *10*, 676-690.

51. Abraham, M. J.; Murtola, T.; Schulz, R.; Páll, S.; Smith, J. C.; Hess, B.; Lindahl, E., GROMACS: High performance molecular simulations through multi-level parallelism from laptops to supercomputers. *SoftwareX* **2015,** *1-2*, 19-25.

52. Melo, M. N.; Ingolfsson, H. I.; Marrink, S. J., Parameters for Martini sterols and hopanoids based on a virtual-site description. *Journal of Chemical Physics* **2015,** *143*.

53. de Jong, D. H.; Baoukina, S.; Ingólfsson, H. I.; Marrink, S. J., Martini straight: Boosting performance using a shorter cutoff and GPUs. *Computer Physics Communications* **2016,** *199*, 1-7.

54. Bussi, G.; Donadio, D.; Parrinello, M., Canonical sampling through velocity rescaling. *Journal of Chemical Physics* **2007,** *126*.

55. Berendsen, H. J. C.; Postma, J. P. M.; van Gunsteren, W. F.; DiNola, A.; Haak, J. R., Molecular dynamics with coupling to an external bath. *The Journal of Chemical Physics* **1984,** *81*, 3684-3690.

56. Parrinello, M.; Rahman, A., Polymorphic transitions in single crystals: A new molecular dynamics method. *Journal of Applied Physics* **1981,** *52*, 7182-7190.

57. Marrink, S. J.; Risselada, J.; Mark, A. E., Simulation of gel phase formation and melting in lipid bilayers using a coarse grained model. *Chem Phys Lipids* **2005,** *135*, 223-244.

58. Kusube, M.; Matsuki, H.; Kaneshina, S., Thermotropic and barotropic phase transitions of N-methylated dipalmitoylphosphatidylethanolamine bilayers. *Biochim Biophys Acta* **2005,** *1668*, 25-32.

59. Ingolfsson, H. I.; Melo, M. N.; van Eerden, F. J.; Arnarez, C.; Lopez, C. A.; Wassenaar, T. A.; Periole, X.; de Vries, A. H.; Tieleman, D. P.; Marrink, S. J., Lipid Organization of the Plasma Membrane. *Journal of the American Chemical Society* **2014,** *136*, 14554-14559.

60. Marrink, S. J.; Risselada, H. J.; Yefimov, S.; Tieleman, D. P.; de Vries, A. H., The MARTINI force field: Coarse grained model for biomolecular simulations. *Journal of Physical Chemistry B* **2007,** *111*, 7812-7824.

61. Huang, J.; Buboltz, J. T.; Feigenson, G. W., Maximum solubility of cholesterol in phosphatidylcholine and phosphatidylethanolamine bilayers. *Biochim. Biophys. Acta* **1999,** *1417*, 89-100.

62. Di Natale, F. Maestro workflow conductor (maestrowf). https://github.com/LLNL/maestrowf.

63. Davis, J. H.; Clair, J. J.; Juhasz, J., Phase equilibria in DOPC/DPPC-d62/cholesterol mixtures. *Biophys J* **2009,** *96*, 521-539.

64. Veatch, S. L.; Keller, S. L., Separation of liquid phases in giant vesicles of ternary mixtures of phospholipids and cholesterol. *Biophys J* **2003,** *85*, 3074-3083.

65. Cicuta, P.; Keller, S. L.; Veatch, S. L., Diffusion of liquid domains in lipid bilayer membranes. *J Phys Chem B* **2007,** *111*, 3328-3331.

66. Uppamoochikkal, P.; Tristram-Nagle, S.; Nagle, J. F., Orientation of Tie-Lines in the Phase Diagram of DOPC/DPPC/Cholesterol Model Biomembranes. *Langmuir* **2010,** *26*, 17363-17368.

67. Humphrey, W.; Dalke, A.; Schulten, K., VMD: Visual molecular dynamics. *J MOL GRAPHICS* **1996,** *14*, 33.

68. Lukat, G.; Kruger, J.; Sommer, B., APL@Voro: a Voronoi-based membrane analysis tool for GROMACS trajectories. *J Chem Inf Model* **2013,** *53*, 2908-2925.

69. Arnarez, C.; Webb, A.; Rouviere, E.; Lyman, E., Hysteresis and the Cholesterol Dependent Phase Transition in Binary Lipid Mixtures with the Martini Model. *J Phys Chem B* **2016,** *120*, 13086-13093.

70. Wang, Y.; Gkeka, P.; Fuchs, J. E.; Liedl, K. R.; Cournia, Z., DPPC-cholesterol phase diagram using coarse-grained Molecular Dynamics simulations. *Biochim Biophys Acta* **2016,** *1858*, 2846-2857.

71. Uline, M. J.; Schick, M.; Szleifer, I., Phase behavior of lipid bilayers under tension. *Biophys J* **2012,** *102*, 517-522.

72. Marsh, D., *Handbook of lipid bilayers*. 2 ed.; CRC Press: 2013.

73. Rodgers, J. M.; Sorensen, J.; de Meyer, F. J.; Schiott, B.; Smit, B., Understanding the phase behavior of coarse-grained model lipid bilayers through computational calorimetry. *J Phys Chem B* **2012,** *116*, 1551-1569.

74. Nagai, T.; Ueoka, R.; Okamoto, Y., Phase Behavior of a Lipid Bilayer System Studied by a Replica-Exchange Molecular Dynamics Simulation. *Journal of the Physical Society of Japan* **2012,** *81*, 024002.

75. Heftberger, P.; Kollmitzer, B.; Rieder, A. A.; Amenitsch, H.; Pabst, G., In situ determination of structure and fluctuations of coexisting fluid membrane domains. *Biophys J* **2015,** *108*, 854-862.

76. Veatch, S. L.; Soubias, O.; Keller, S. L.; Gawrisch, K., Critical fluctuations in domain-forming lipid mixtures. *Proc Natl Acad Sci U S A* **2007,** *104*, 17650-17655.
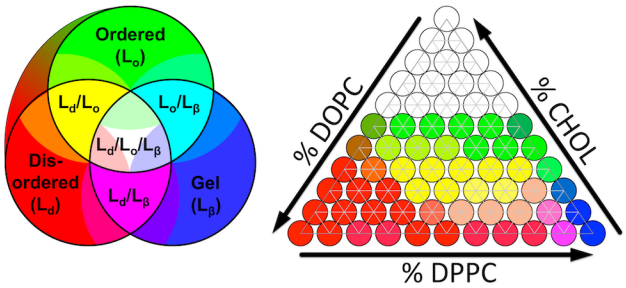
For Table of Contents Only